GEOMAGNETIC FIELD PERTURBATIONS CAUSED BY THE TURBULENT FLOW OF A CONDUCTING FLUID AROUND THE BALL

© 2025 V. V. Surkov[a], *, E. V. Semyonov[b], V. M. Sorokin[c], A. K. Yashchenko[c]

[a]*Schmidt Institute of Physics of the Earth of the Russian Academy of Science? Moscow*

[b]*Shirshov Institute of Oceanology of the Russian Academy of Science, Moscow*

[c]*Pushkov Institute of Terrestrial Magnetism, Ionosphere and Radio Wave Propagation of the Russian Academy of Sciences, Moscow, Troitsk*

**e-mail: surkovvadim@yandex.ru*

Received March 13, 2025

Revised May 06, 2025

Accepted May 22, 2025

Abstract. In this study the perturbations of an external magnetic field produced by a turbulent flow of a conductive incompressible liquid flowing around a solid dielectric ball are considered. The fluid flow is calculated in the approximation of the RANS model, which takes into account the effects of turbulent viscosity. The COMSOL multiphysical simulation platform was used for numerical modelling of hydrodynamic and magnetic perturbations. The solution of the problem is obtained for an arbitrary orientation of the external magnetic field. The angular distribution of magnetic perturbations, as well as the decrease of amplitudes of these disturbances with distance, is numerically investigated. The angular distribution of magnetic perturbations, as well as the decrease in the amplitudes of these perturbations with distance, is numerically studied. The directions of maximum magnetic perturbations are determined. The area near the turbulent wake is being investigated in detail. Approximate asymptotic laws of decreasing magnetic perturbations are derived as functions of the distance to the ball center. The magnetic perturbations caused by laminar and turbulent regimes of fluid flow around a ball are compared.

Keywords: *geomagnetic perturbations, conductive fluid, laminar flow, turbulent flow, turbulent wake*

DOI: 10.31857/S00167940250513e4

1. INTRODUCTION

The motion of conducting media in a magnetic field is accompanied by the generation of induction electric currents and magnetic field perturbations [Landau and Lifshitz, 1982]. This effect

is caused by the action of magnetic forces on moving electric charges in a conducting medium. Under natural conditions, perturbations of the Earth's magnetic field have been observed, caused both by the motion of tsunami waves in salty ocean water, which has a large electrical conductivity, and by the propagation of seismic waves on land in the conductive layers of the Earth [Surkov and Hayakawa, 2014]. Geomagnetic disturbances can be generated by wind waves in the ocean, tidal currents, internal and ship waves, etc. [Weaver, 1965; Sanford, 1971]. Especially notable geomagnetic disturbances are produced by tsunami waves, which involve a huge mass of water and have a large transverse extent [Manoj and Maus, 2011; Toh et al., 2011]. Numerical modeling of tsunami waves shows that geomagnetic disturbances on the ocean and land surfaces can reach tens of nanotesla [Wang and Liu, 2013; Zhang et al., 2014]. Tsunami waves are accompanied by the generation of acoustic-gravity waves in the atmosphere, which create an additional effect of geomagnetic perturbations associated with the excitation of currents in the ionospheric plasma [Artru et al., 2005; Sorokin et al., 2019; Sorokin et al., 2019].

Small local geomagnetic perturbations can occur when ships move in seawater. The cause of these perturbations is the generation of electric currents in conductive seawater during ship hull streamline [Yaakob et al., 2011, Zhu et al]., 2015 . The structure of the magnetic perturbation field near a body moving in a conducting fluid depends significantly on the velocity distribution in the fluid flow around the body. There are several simple analytical solutions describing the laminar flow regime of an infinite circular cylinder, ball, and ellipsoid moving in an unbounded liquid incompressible medium [Landau and Lifshitz, 1986]. If the body moves in a liquid half-space, the problem becomes much more complicated, since in this case it is necessary to take into account the boundary conditions not only on the body surface but also on the free surface of the liquid [Havelock, 1928; Sretensky, 1997; Arzhannikov and Kotelnikov, 2016].

Analytical solutions for the magnetic perturbations arising during stationary laminar flow of a solid dielectric ball in a conducting incompressible fluid were obtained in [Dorman and Mikhailov, 1952; Surkov et al., 2017]. In these studies, it was shown that geomagnetic perturbations decrease at large distances l' from the center of the balloon proportionally r^{-2} , and electrical perturbations as r^{-3} . Moreover, the angular distribution of these perturbations depends significantly on the angle between the vectors of the ball's velocity and the unperturbed magnetic field. For the case of ball motion in a liquid half-space, an approximate solution has been found [Surkov et al., 2018] . In this case, the asymptotic laws of decreasing electromagnetic perturbations with distance remain the same, but the spatial structure of the fields becomes more complicated.

The purpose of this paper is to generalize the results of previous studies to the case of turbulent flow of a solid dielectric ball with a conducting fluid in a geomagnetic field. For this purpose, the numerical solution of the problem is considered, with special attention paid to the turbulent wake

region. On the basis of this solution, the distribution of magnetic perturbations and their dependence on the distance to the center of the ball are evaluated, and the results of numerical calculations are compared with the analytical solution of the problem in the laminar flow approximation.

2. PROBLEM FORMULATION

Consider a dielectric non-magnetic ball of radius R moving with constant velocity $\mathbf{V}_0$ in a conducting homogeneous fluid located in a homogeneous magnetic field with induction $\mathbf{B}_0$, directed at an angle β to the ball velocity vector. We will investigate small perturbations $\mathbf{b}$ of the magnetic field ($|\boldsymbol{b}| \ll |\boldsymbol{B}_0|$). These perturbations are caused by electric currents that are generated in the flow of fluid flowing around the ball.

Let us move to a frame of reference in which the ball is at rest and the distributions of the mass velocity of the fluid $\mathbf{V}$, magnetic $\mathbf{b}$ and electric $\mathbf{E}$ perturbations are stationary, i.e., do not depend on time. Then Maxwell's equations take the form:

$$\nabla \times \mathbf{b} = \mu_0 \sigma \left(\mathbf{E} + \mathbf{V} \times \mathbf{B}_0 \right), \tag{1}$$

$$\nabla \times \mathbf{E} = \mathbf{0}, \tag{2}$$

where μ_0 is the magnetic constant, and we consider the electrical conductivity of the fluid σ to be a constant value. The components of electromagnetic perturbations $\mathbf{b}'$ and $\mathbf{E}'$ for a stationary observer, relative to which the ball moves, can be found by means of the electromagnetic field transformation. In the nonrelativistic limit this transformation has the form: $\mathbf{b}' \approx \mathbf{b}$ and $\mathbf{E}' \approx \mathbf{E} + \mathbf{V} \times \mathbf{B}_0$.

It should be noted that in the region of turbulent fluid flow its velocity experiences random fluctuations. Perturbations of electric and magnetic fields caused by the fluid motion are also subject to random fluctuations. The relationship between the averaged values of these perturbations and the average velocity of turbulent motion $\mathbf{V}$ is found by averaging equations (1) and (2). Taking into account the linearity of these equations and the constancy of the parameters σ and $\mathbf{B}_0$, we obtain that the form of the equations for the average values remains the same. Therefore further, $\mathbf{V}$ $\mathbf{E}$ and $\mathbf{b}$ in the field of turbulent flow will denote the averaged values of these quantities.

Let's take the rotor from both parts of the equation, and using the equation together with the equality $\nabla \cdot \mathbf{b} = \mathbf{0}$, we obtain:

$$\nabla^2 \mathbf{b} = -\mu_0 \sigma \nabla \times \left(\mathbf{V} \times \mathbf{B}_0 \right). \tag{3}$$

Inside the ball, the equation $\nabla^2 \mathbf{b} = 0$ is satisfied since the ball is dielectric and non-magnetic. The components of the magnetic perturbation must be continuous on the surface of the ball, moreover, the solution of Maxwell's equations must be finite at the center of the ball and at infinity.

In the following we use the spherical coordinate system r, θ, φ with the origin at the center of the ball and the polar axis z, directed opposite to the vector $\mathbf{V}_0$ (Fig.1). The velocity field at laminar flow of an ideal incompressible fluid around the ball has the form [Landau and Lifshitz, 1986] :

$$\mathbf{V} = \left[\frac{3(\mathbf{r}\mathbf{V}_0)\mathbf{r}}{r^2} - \mathbf{V}_0 \right] \frac{R^3}{2r^3} - \mathbf{V}_0 . \tag{4}$$

Here $\mathbf{r}$ denotes the radius-vector shown in Fig. 1.

Fig. 1.

The solution of Maxwell's equation with the above boundary conditions and laminar velocity field , obtained in [Surkov et al, 2017; Surkov et al]., 2018 has the form:

$$\mathbf{b} = \frac{\mu_0 \sigma}{8\pi} \left\{ \mathbf{r} S(\mathbf{r}) + \nabla S(\mathbf{r}) \frac{R^2}{5} \right\}, \quad \mathbf{E} = \nabla \frac{\mathbf{r} \cdot (\mathbf{p} \times \mathbf{B}_0)}{8\pi r^3},$$
$$S(\mathbf{r}) = \frac{\mathbf{p} \cdot \mathbf{B}_0}{r^3} - \frac{3(\mathbf{p} \cdot \mathbf{r})(\mathbf{B}_0 \cdot \mathbf{r})}{r^5}. \tag{5}$$

Here the vector $\mathbf{p} = 2\pi R^3 \mathbf{V}_0$ makes sense of the hydrodynamic dipole moment. From the formulas we can see that at large distances, when $r \gg R$, the magnetic and electric fields asymptotically decrease: $\mathbf{b} \propto r^{-2}$ $\mathbf{E} \propto r^{-3}$.

At large Reynolds numbers $\mathrm{Re} = \rho R V_0 / \eta$, the streamline of the balloon becomes turbulent and the formula for the velocity field is no longer applicable. Setting, for example, the radius of the ball $R = 5$ m, the velocity of the fluid flow $V_0 = 1$ m/s, the density of the fluid $\rho = 10^3$ kg/m^3, the molecular viscosity $\eta = 8.9 \cdot 10^{-4}$ Pa· s, we obtain that . $\mathrm{Re} = 5 \cdot 10^6$

The turbulent fluid flow was calculated numerically using $k - \varepsilon$ RANS model [Rodi, 2017] . The hydrodynamic equations were solved numerically in the multiphysics simulation program COMSOL. The stationary solution of the problem was found by the method of establishment, i.e. as the limit to which the solution of the unsteady problem with zero initial velocity of motion tends asymptotically at large time, then tending to a constant. To calculate the hydrodynamic and magnetic perturbations, the above parameter values were chosen, as well as the fluid conductivity $\sigma = 4$ cm/m and the induction of the external magnetic field $B_0 = 5 \cdot 10^{-5}$ Tesla. The turbulent viscosity was calculated at each point in a self-consistent manner using the RANS model equations. The size of the computational domain is $1000 \times 500 \times 500$ meters.

In the Cartesian coordinate system (x, y, z) , the center of the ball is located at $(0, 0, -250$ м$)$, the fluid flow runs along the axis z . On the lateral surface of the calculation area the conditions of non-flow and equality to zero of the tangential component of viscous stress are set. On the surface of

the ball the boundary condition of adhesion is set. In other words, on the surface of the ball the velocity of the fluid is considered to be equal to the velocity of the corresponding point of the ball. For electromagnetic field calculations, the magnetic perturbation on the surface of the ball is assumed to be continuous.

3. DISTRIBUTION OF MAGNETIC FIELD PERTURBATIONS AROUND THE BALL

The analysis of the solution shows that at large distances from the ball the radial component of the magnetic perturbation dominates. The results of calculations of the b_r component are presented in Fig. 2 at different angles β between the vector $\mathbf{B}_0$ and the axis z . The two-dimensional distributions of b_r in the $y = 2R$ plane at different orientations of the external magnetic field are depicted here. The general picture of distributions b_r has the form of four "petals" for both laminar and turbulent character of fluid flows. However, the appearance of these "lobes" is different. The left panels, (*a*) and (*c*), correspond to laminar flow of the ball, the right panels, (*b*) and (*d*), correspond to turbulent flow. In this and subsequent figures, for the case of turbulent fluid flow, b_r means the averaged value of magnetic perturbation. The upper panels, (*a*) and (*b*), show the distribution of b_r , when the vectors $\mathbf{B}_0$ and $\mathbf{V}_0$ are oppositely directed, while in the lower panels, (*c*) and (*d*), they are orthogonal.

Fig. 2.

Comparison of the figures in the upper and lower panels shows that the direction of the external magnetic field significantly affects both the amplitude and the structure of the magnetic field, i.e., the location of maxima and minima. At $\beta = 0^\circ$, as one would expect, the magnetic field distribution is symmetric about the ball velocity vector. At $\beta = 90^\circ$, the projection vectors b_r at symmetric points to the left and right of the vertical axis of symmetry differ only in sign. Therefore, a maximum on one side corresponds to a symmetrically located minimum on the other side.

The largest difference in the figures, noticeable in the bottom panel, is due to the presence of the turbulent trace shown in gray in the lower right panel. In the vicinity of this trace, sharp variations are seen b_r , which are absent in laminar flow (lower left panel). It should be noted that in this region the calculation we used describes only the mean flow velocity, which in reality is superimposed by different-scale turbulent fluctuations. Therefore, near the turbulent wake, Fig. *2g* describes the distribution of only the mean values of b_r .

Fig. 3.

Let us compare the degrees of decrease of the magnetic perturbation with distance outside and inside the turbulent footprint region. In Fig. 3 shows the dependences of the magnetic perturbation modulus on the distance to the ball surface calculated along the ray drawn at an angle $\theta = 45°$ to the axis Z for different angles of inclination β of the magnetic field relative to the direction of velocity of the impinging fluid flow.

As can be seen from this figure, the averaged magnetic perturbation decreases more slowly with distance in turbulent flow around the balloon. Away from the balloon, the logarithmic dependence of the perturbation on distance becomes almost linear, i.e., the decrease b follows a step law. At $\beta = 90°$ and large distances from the balloon: $b \propto r^{-n}$, where $n \approx 1.65$ for turbulent flow and $n \approx 1.9$ for laminar flow. At distances of about $250 - 350$ m, the turbulent type of disturbance becomes larger than the laminar type by almost an order of magnitude. Obviously, this regularity is related to the different character of the decrease with distance of the liquid velocity in laminar and turbulent flows. Apparently, the energy transferred to the fluid by the ball moving with constant velocity is greater in turbulent flow, and, accordingly, the energy transformed into electromagnetic perturbations is greater.

A comparison of the plots in the left and right panels of Fig. 3 shows that the magnetic perturbations are larger when the angle of inclination of the external magnetic field is $\beta = 90°$. The same trend can be seen in Fig. 4, which shows the dependence of b on the polar angle θ . This figure also shows that for all angles β , the largest perturbations are achieved in the range of values θ from zero to $5°$. The same approximate trend can be seen in Fig. *2d*. Thus the region of the largest magnetic perturbations is located behind the ball near the axis z.

Fig. 4.

Figure 5 illustrates the dependence of the magnetic perturbations on the distance to the balloon in this region. The left and right panels show the cases where the unperturbed magnetic field $\mathbf{B}_0$ is parallel and perpendicular to the velocity of the ball $\mathbf{V}_0$, respectively. From the plots in Fig. 5, it can be seen that in turbulent flow of the balloon (solid line), the magnetic perturbations are, first, much larger than in laminar flow (dashed line) and, second, decrease more slowly with distance in the region behind the balloon.

Fig. 5.

4. DISTRIBUTION OF MAGNETIC PERTURBATIONS IN A TURBULENT WAKE

To analyze this difference in more detail, let us consider the features of fluid flow and magnetic perturbations near the turbulent wake. Fig. 6 shows the dependence of the longitudinal z -component of the fluid velocity relative to the ball in the turbulent wake along the z axis as a function of the

distance $z - z_0$ to the center of the ball. Figure 6 shows that in the distance range $r = z - z_0 = 10 \div 200$ m the graph is approximately rectilinear. Given the logarithmic scale of the graph, we obtain that the following approximation is valid in this range $V_0 - V_z \propto r^{-0.66}$. Note that in theory the perturbations of the longitudinal velocity in the turbulent wake decrease with distance in proportion to $r^{-2/3}$ [Landau and Lifshitz, 1986].

Fig. 6.

For distances $r > 500$ m, the graph in Fig. 6 is close to a linear dependence. In this range of distances the following approximation can be used: $V_0 - V_z \propto r^{-2.8}$, which is close to the dependence r^{-3} . Note that a similar asymptotic law follows from equation (3) describing the laminar flow of the balloon.

Fig. 7 shows the perturbations of the longitudinal velocity along the axis x , i.e., across the turbulent wake, at different distances from the balloon. Thus, the characteristic transverse scale of the turbulent trace is much smaller than its longitudinal size, which agrees with both observations and theoretical estimates [Landau and Lifshitz, 1986]. Numerical calculations show that the condition $V_0 - V_z >> V_x$, i.e., the transverse component of the velocity becomes small compared to the longitudinal component, is satisfied at distances from the ball exceeding approximately 20 m. The transverse component of the velocity becomes small compared to the longitudinal component.

Fig. 7.

Fig. 8 shows the projection of the magnetic perturbation b_z on a straight line parallel to the axis z in the turbulent wake as a function of the distance from the center of the balloon. The straight line with coordinates $x = 5$ m and $y = 0$, since $b_z = 0$ is on the axis $x = y = 0$, is chosen for the calculations. For distances $r = z - z_0 = 10 \div 150$ m and at $r > 250$ m the graph in Fig. 8 can be approximated by two straight lines. Therefore, in the first range of distances we can use an approximate dependence of the form $b_z \propto r^{-0.42}$, and at $r > 250$ m we obtain: $b_z \propto r^{-2.89}$, which is close to . r^{-3}

Fig. 8.

A comparison of the asymptotic laws of decreasing perturbations of the longitudinal velocity and magnetic perturbation b_z , shown in Figures 6 and 8, shows that in the region of the turbulent wake (in the range $10 < r < 150$ m), the degree exponent in the decreasing law $V_0 - V_z$ is larger than

that of b_z , while in the region $r > 150$ m both quantities decrease almost equally, i.e., approximately in proportion to r^{-3}.

Figure 9 shows the distribution of the b_z component across the turbulent trace behind the ball at different distances to its center. The width of this distribution is small compared to the length of the turbulent wake, but is slightly larger than the width of the distribution of longitudinal velocity perturbations shown in Fig. 7. The bipolar appearance of the plots in Fig. 9 is due to the fact that the transverse velocity components have opposite signs on different sides of the axis z . This leads to a change of signs of z -component of the extrinsic current density $\sigma\left(\mathbf{V}\times\mathbf{B}_0\right)$ in equation (1) with a subsequent change of signs of the projections of the magnetic perturbation on the axis x.

Fig. 9.

The distribution of the projection b_x , perpendicular to the turbulent wake, is shown in Fig. 10. The amplitude of this component of the magnetic perturbation is smaller than that of b_z , and decreases rapidly with distance from the ball. The width of this distribution significantly exceeds the characteristic transverse dimension of the turbulent wake.

Fig. 10.

5. DISCUSSION AND CONCLUSION

The above studies of the geomagnetic field perturbations produced by a moving solid dielectric body in a conducting fluid allowed us to analyze the differences of these perturbations in the laminar and turbulent regimes of balloon flow. In both regimes, the two-dimensional distributions of the radial component of the magnetic perturbation, shown in Fig. 2, have the form of four "petals", i.e., they have some similarity, especially noticeable when the vectors of the ball velocity $\mathbf{V}_0$ and the unperturbed magnetic field $\mathbf{B}_0$ are parallel. The difference becomes more significant when $\mathbf{V}_0$ and $\mathbf{B}_0$ are orthogonal. Solution of the equations by numerical methods shows that in turbulent flow, the magnetic perturbations behind the balloon decrease more slowly with distance. For example, along a ray forming an angle $\theta = 45°$ with the z axis, the averaged magnetic perturbations for turbulent flow decrease at large distances r approximately proportional to r^{-n} , where $n \approx 1.65$. For laminar flow $n \approx 1.9$, which agrees with the analytical solution (5), which gives the value $n = 2$. At relative distances $r/R = 50 - 70$, the turbulent type of magnetic perturbations becomes larger than the laminar type by almost an order of magnitude.

Of greatest interest is the region behind the balloon near the turbulent wake. Calculations show that in the wake region the longitudinal velocity perturbations $V_0 - V_z$ depend nonlinearly on the

distance to the ball $r = z - z_0$. For relative distances $r/R = 2 - 40$, the following approximation is valid $V_0 - V_z \propto r^{-0.66}$. This law is close to the theoretical relation according to which the velocity perturbations in the turbulent wake decrease with distance proportionally to $r^{-2/3}$ [Landau and Lifshitz, 1986]. For distances $r/R > 100$ one can use an approximation of the form: $V_0 - V_z \propto r^{-2.8}$, which is close to the dependence r^{-3} . From formula (4) we can see that this asymptotic law is valid for laminar flow of the ball. Therefore, this result implies a natural transition from the turbulent regime to the laminar regime at large distances from the ball.

Note also that in directions transverse to the turbulent wake, the velocity perturbations decrease rapidly with distance, which is consistent with theory. Moreover, at distances from the ball exceeding approximately $r/R = 4$ the transverse component of the velocity V_x becomes small compared to the longitudinal velocity perturbations.

Magnetic perturbations reach their maximum values near the turbulent wake when $\mathbf{B}_0$ is perpendicular to $\mathbf{V}_0$, i.e., the wake axis. Numerical calculations show that in the wake region the magnetic perturbations, as well as the longitudinal velocity perturbations, depend nonlinearly on the distance to the ball $r = z - z_0$. For distances $r/R = 2 - 30$, the calculation results can be approximated by a dependence of the form: $b_z \propto r^{-0.42}$. For distances $r/R > 50$, the approximate asymptotic law is of the form: $b_z \propto r^{-2.89}$, which is close to r^{-3} . It should be noted here that such a decreasing law can be obtained from formula (5) describing the magnetic perturbations at laminar flow of the ball, if we take into account that in the case considered above the vectors $\mathbf{p}$ and $\mathbf{B}_0$ are orthogonal.

The width of the distribution of magnetic perturbations in the direction transverse to the turbulent wake is, on the one hand, small compared to the length of the wake, but, on the other hand, larger than the width of the wake itself. Such transverse expansion of magnetic perturbations in comparison with velocity perturbations is due to the fact that magnetic perturbations are defined by some integral over the distribution of the whole set of currents generated due to the motion of the conducting fluid, i.e., they are an integral effect determined not only by the currents in the turbulent trace, but by all currents in the fluid volume.

Thus, the largest differences in magnetic perturbations in laminar and turbulent flow regimes are mainly concentrated behind the ball in the region of the turbulent wake. These differences become especially noticeable when the velocity vectors of the balloon and the unperturbed geomagnetic field are orthogonal. In this case, the magnetic perturbations decrease with distance along the turbulent

wake much slower compared to the laminar flow regime. These features of magnetic perturbations refer to their average values, since only averaged turbulent flow velocities were considered in this work. In reality, magnetic perturbations in the trace region may experience fluctuations associated with turbulent pulsations of fluid flows.

REFERENCES

1. *Dorman L.I., Mikhailov Yu.M.* Investigation of electromagnetic phenomena during the flow of bodies in a conducting liquid in a magnetic field // JETF. V. 43. P. 752-762. 1952.

2. *Landau L.D., Lifshits E.M.* Electrodynamics of continuous media / M.: Nauka, 620 p. 1982.

3. *Landau L.D., Lifshits E.M.* Hydrodynamics / M.: Nauka, 736 p. 1986.

4. *Sorokin V.M., Yashchenko A.K., Surkov V.V.* Generation of geomagnetic disturbances in the ionosphere by a tsunami wave // Geomagnetism and aeronomy. V. 59. No. 2. P. 236-248. 2019. https://doi.org/10.1134/S0016794019020135 .

5. *Sretensky L.N.* Theory of wave motions, 2nd ed., reprint. and add., M.: Nauka, Glav. Ed. fiz.-mat. lit., 816 p., 1977.

6. *Surkov V.V., Sorokin V.M., Yashchenko A. K.* Geomagnetic disturbances caused by the motion of a ball in a conducting liquid // News of higher educational institutions. Radiophysics. V. 60. No. 7. P. 617-626. 2017.

7. *Arzhannikov A.V., Kotelnikov I.A*. Excitation of ship waves by a submerged object: new solution to the classical problem // Phys. Rev. E. V. 94. 023103. 2016. https://doi.org/10.1103/PhysRevE.94.023103.

8. *Artru J., Ducic V., Kanamori H., Lognonne P., Murakami M.* Ionospheric detection of gravity waves induced by tsunamis // Geophys. J. Int. V. 160. P. 840–848. 2005.

9. *Havelock T.H*. The wave pattern of a doublet in a stream // Proc. Roy. Soc. Lond. (A). V. 121. P. 515–523. 1928.

10. *Manoj C., Maus S.* Observation of magnetic fields generated by tsunamis // EOS. V. 92. № 2. P. 13−14. 2011.

11. *Rodi W*. Turbulence models and their application in hydraulics: A state-of-the-art review, 3rd ed., ed. Rodi W., Routledge, 2017.

12. *Sanford T.B*. Motionally induced electric and magnetic fields in the sea // J. Geophys. Res. V. 76. P. 3476–3492. 1971.

13. *Sorokin V.M., Yashchenko A.K., Surkov V.V*. Geomagnetic field perturbations resulted from tsunami wave impact on the ionosphere // Progress in Electromagnetics Research BV. 85. P. 49–63. . 2019. https://doi.org/10.2528/PIERB19050201.

14. *Surkov V., Hayakawa M.* // Ultra and Extremely Low Frequency Electromagnetic Fields, Springer Geophysics Series, XVI, Springer, 486 p. 2014. https://doi.org/10.1007/978-4-431-54367-1.

15. *Surkov V.V., Sorokin V.M., Yashchenko A.K.* Perturbations of ambient magnetic field resulted from a ball motion in a conductive liquid half-space // Progress in Electromagnetics Research B. V. 80. P. 113–131. 2018.

16. *Toh H., Satake K., Hamano Y., Fujii Y., Goto T.* Tsunami signals from the 2006 and 2007 Kuril earthquakes detected at a seafloor geomagnetic observatory // J. Geophys. Res. V. 116. N B2. 2011.

17. *Wang B., Liu H.* Space-time behaviour of magnetic anomalies induced by tsunami waves in open ocean // Proc. Roy. Soc. A. V. 469. № 257. 2013.

18. *Weaver J.T.* Magnetic variations associated with ocean waves and swells // J. Geophys. Res. V. 70. P. 1921–1929. 1965.

19. *Yaakobi O., Zilman G., Miloh T.* Detection of the electromagnetic field induced by the wake of a ship moving in a moderate sea state of finite depth // J. Eng. Math. V. 70. P. 17–27. 2011.

20. *Zhang L., Utada H., Shimizu H., Baba K., Maeda T.* Three-dimensional simulation of the electromagnetic fields induced by the 2011 Tohoku tsunami: Simulation of the EM fields of tsunami // J. Geophys. Res. V. 119. № 1. P. 150–168. 2014.

21. *Zhu X.J., Du C.P., Xia M.Y.* Modeling of magnetic field induced by ship wake // 2015 IEEE International Conference on Computational Electromagnetics, Hong Kong, China. P. 374–376. 2015. https://doi.org/10.1109/COMPEM.2015.7052667.

FIGURE CAPTIONS

Fig. 1. Current lines in laminar flow of a ball and spherical coordinate system.

Fig. 2. Two-dimensional distributions of the radial component of the magnetic perturbation b_r in the plane $y = 2R$ for laminar and turbulent flowing of the ball and different angles of inclination of the unperturbed magnetic field $\mathbf{B}_0$ relative to the direction of velocity of the impinging fluid flow. The left column of panels, (*a)* and (*c*), corresponds to laminar flow, the right column, (*b*) and (*d*), to turbulent flow. The top row of panels, (*a*) and (*b*), are plotted for $\beta = 0°$, and the bottom row, (c) and (d), for $\beta = 90°$. The velocity vector of the balloon is indicated by the white arrow.

Fig. 3. Dependences of the absolute magnitude of the magnetic perturbation on the distance $r - R$ to the ball surface along the ray forming the angle $\theta = 45°$ with the axis z . The ray is drawn in the plane of vectors $\mathbf{B}_0$ and $\mathbf{V}_0$. On the left panel $\beta = 0°$, on the right panel $\beta = 90°$, the solid and dashed lines correspond to the cases of turbulent and laminar flow regimes of the balloon.

Fig. 4. Dependences of the absolute magnitude of the magnetic perturbation on the polar angle θ in the plane $y = 0$ at a distance of 150 m from the center of the balloon for different angles of inclination β *of* the magnetic field relative to the direction of velocity of the impinging fluid flow. The solid, dashed, dotted, and dashed-dashed lines correspond to the values of the polar angle $\beta = 0°, 30°, 60°, 90°$.

Fig. 5. Dependences of the radial component of the magnetic perturbation on the coordinate z along a straight line parallel to the axis z , with coordinates $x = y = 3R$. The solid line corresponds to turbulent flow and the dashed line to laminar flow. In the left panel $\beta = 0$, in the right panel $\beta = 90°$.

Fig. 6. Dependence of the perturbation of the longitudinal fluid velocity in the turbulent trace behind the balloon on the distance to its center.

Fig. 7. Dependence of the perturbation of the longitudinal velocity across the turbulent trace behind the ball at $y = 0$ and different distances $z - z_0$ to its center. Solid, dashed, dotted and dashed-dotted lines correspond to $z - z_0 = 10, 50, 150, 200$ m.

Fig. 8. Dependence of the longitudinal component of the magnetic perturbation in the turbulent trace behind the ball on the distance to its center. Calculations were performed along a straight line parallel to the axis z , with coordinates $x = 5$ m and $y = 0$. The external magnetic field $\mathbf{B}_0$ is directed along the axis x .

Fig. 9. Dependence of the longitudinal component of the magnetic perturbation b_z across the turbulent trace behind the ball at $y = 0$ and different distances $z - z_0$ to its center. The solid, dashed, dotted, and dashed-dotted lines correspond to the values: $z - z_0 = 10, 50, 150, 200$ m. The external magnetic field $\mathbf{B}_0$ is directed along the axis x .

Fig. 10. Same as Fig. 9, but for the transverse component of the magnetic perturbation.

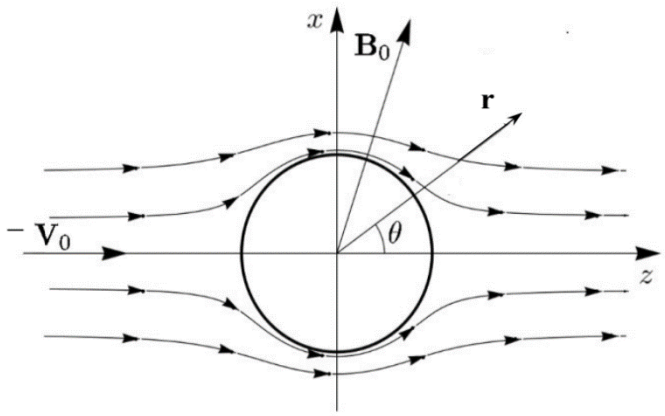

Fig. 1.

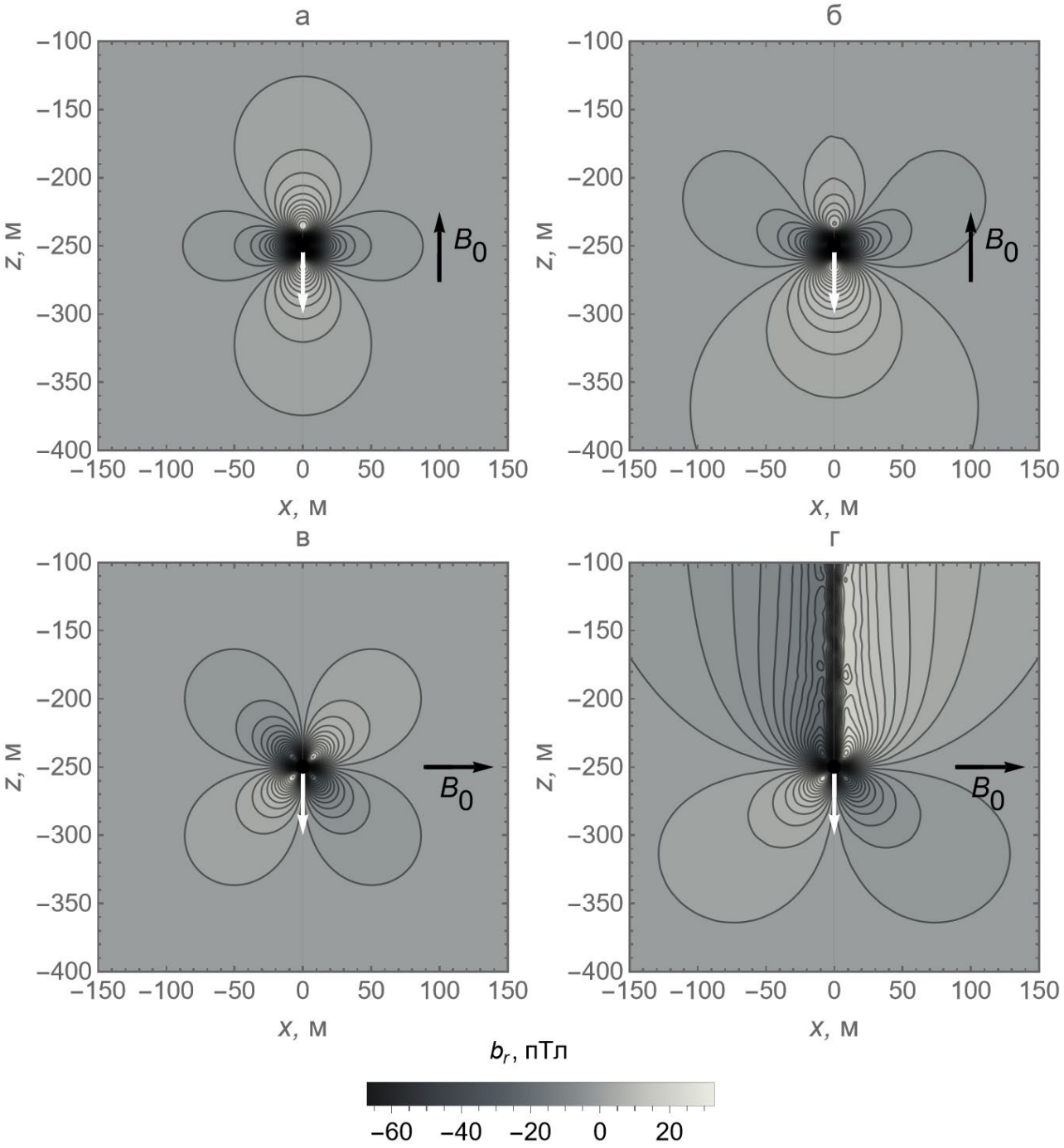
а
б
в
г
z, м
x, м
B0
−100
−150
−200
−250
−300
−350
−400
−150 −100 −50 0 50 100 150
br, пТл
−60 −40 −20 0 20

Fig. 2.

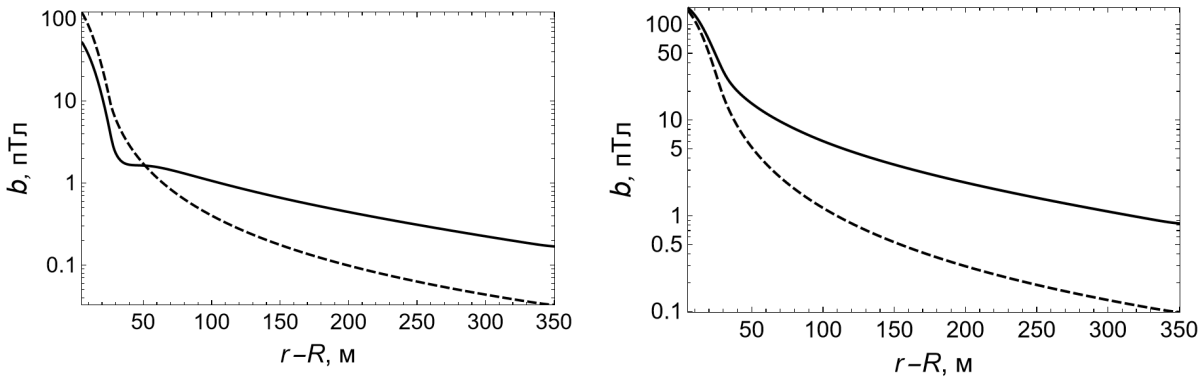
100
10
1
0.1
b, пТл
50
100
150
200
250
300
350
r–R, м
100
50
10
5
1
0.5
0.1
b, пТл
50
100
150
200
250
300
350
r–R, м

Fig. 3.

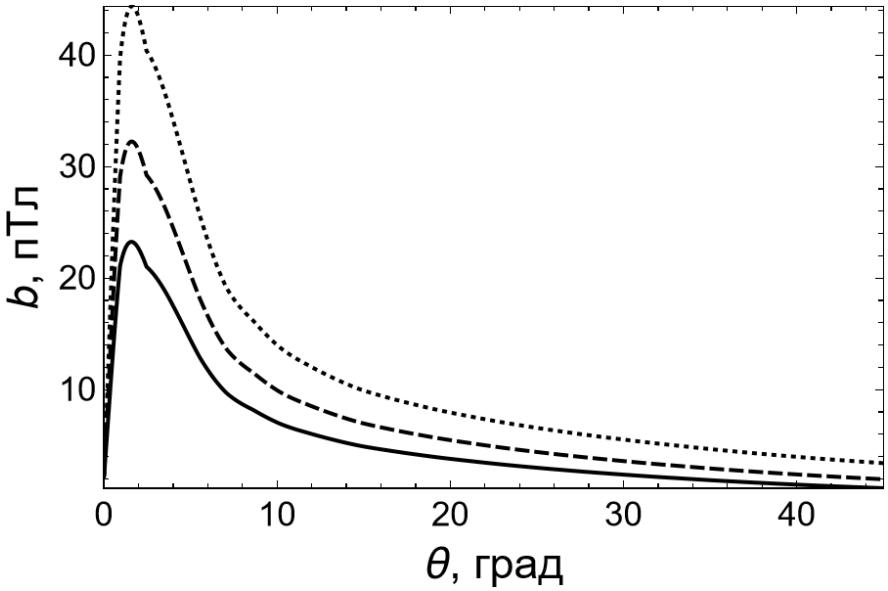
40
30
20
10
b, пТл
0
10
20
30
40
θ, град

Fig. 4.

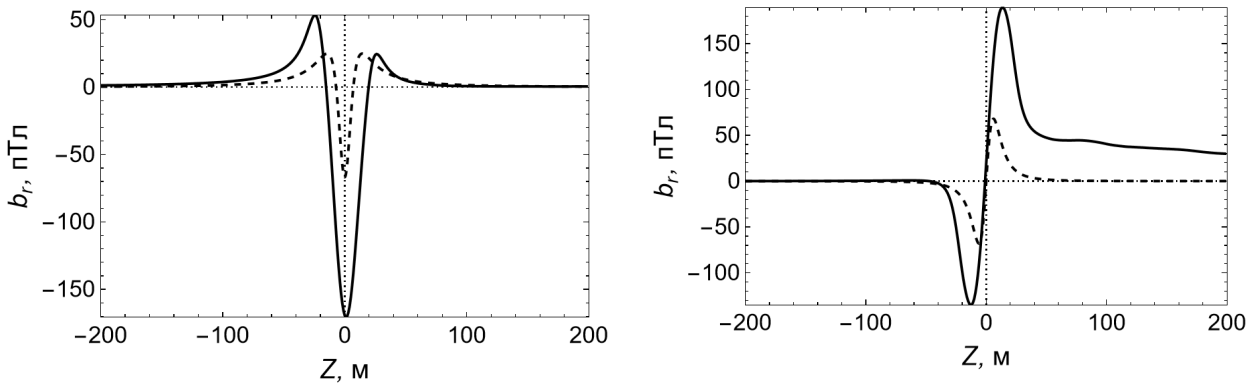

Fig. 5.

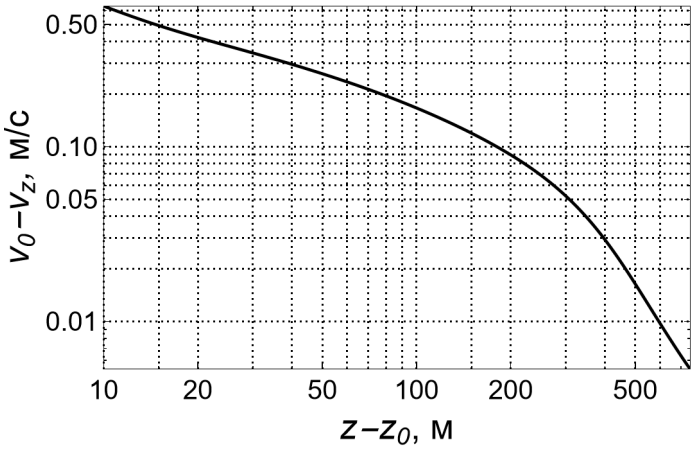

Fig. 6.

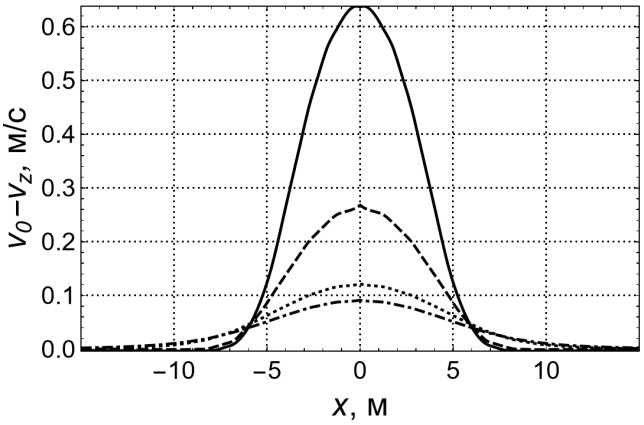

Fig. 7.

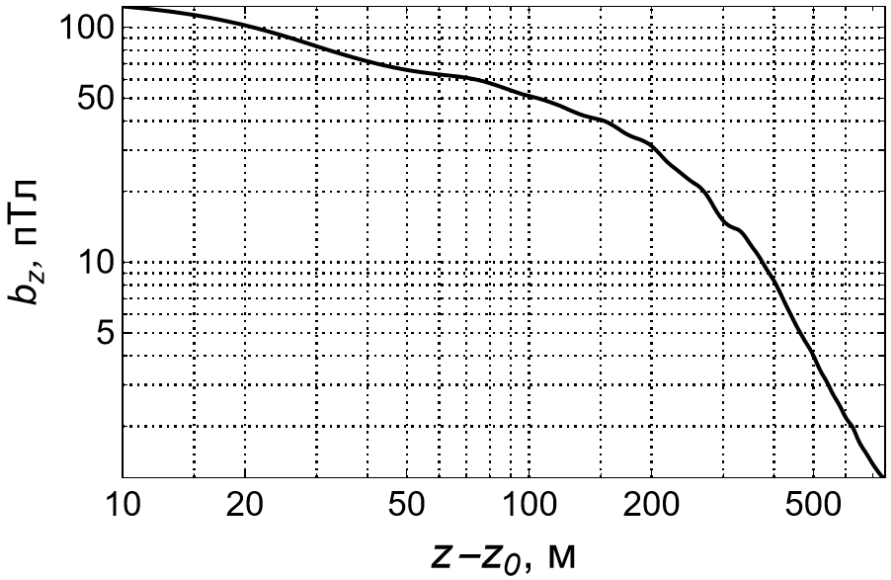
100
50
10
5
b_z, пТл
10
20
50
100
200
500
$z - z_0$, м

Fig. 8.

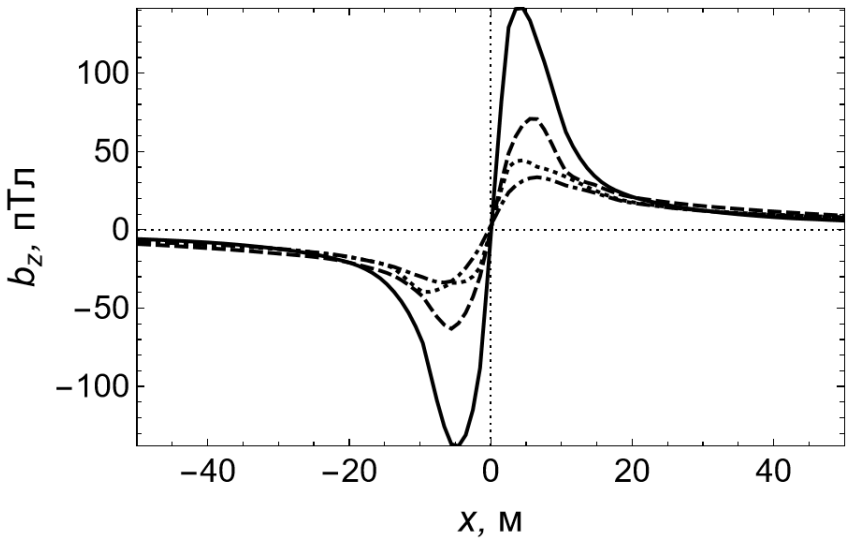
100
50
0
−50
−100
b_z, пТл
−40
−20
0
20
40
x, м

Fig. 9.

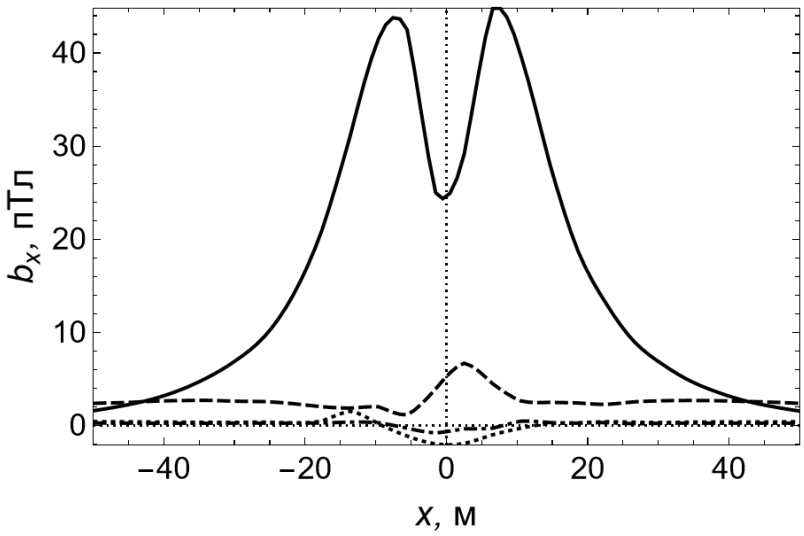

Fig. 10.